Electrostatic Confinement of Aquated Monocationic Gd(III) Complex-Molecules within the Inner Core of Porous Silica Nanoparticles Endows a Highly Efficient T_1 Contrast Agent for Magnetic Resonance Imaging

Riya Mallik,[‡a] Mahmuda Khannam,[‡a] Muktashree Saha,[b] Shivani Marandi,[c] Sachin Kumar,[b] Chandan Mukherjee[a*]

*Corresponding address:

Dr. Chandan Mukherjee, Department of Chemistry, Indian Institute of Technology Guwahati, Guwahati, 781039, Assam, India

Email: cmukherjee@iitg.ac.in

Phone No. +91-361-258-2327

Fax: +91-361-258-2349

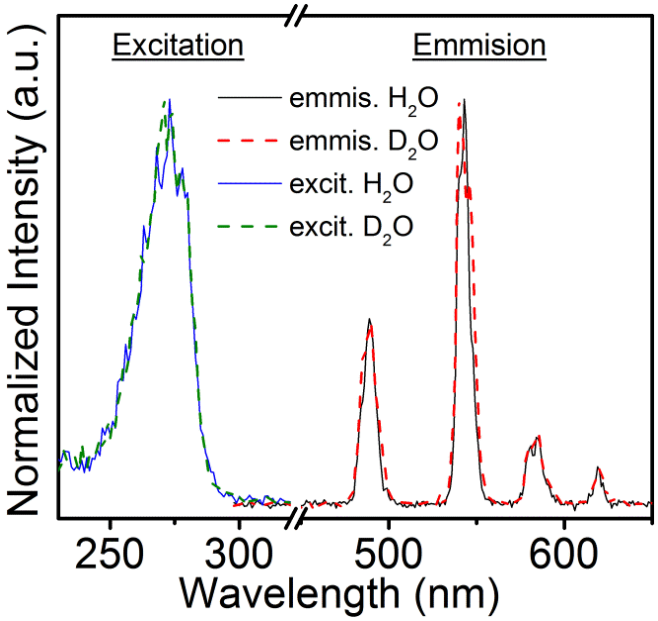

Figure S1. Excitation and emission spectra of complex **2** in H_2O, and in D_2O (0.5 mM, 25 °C).

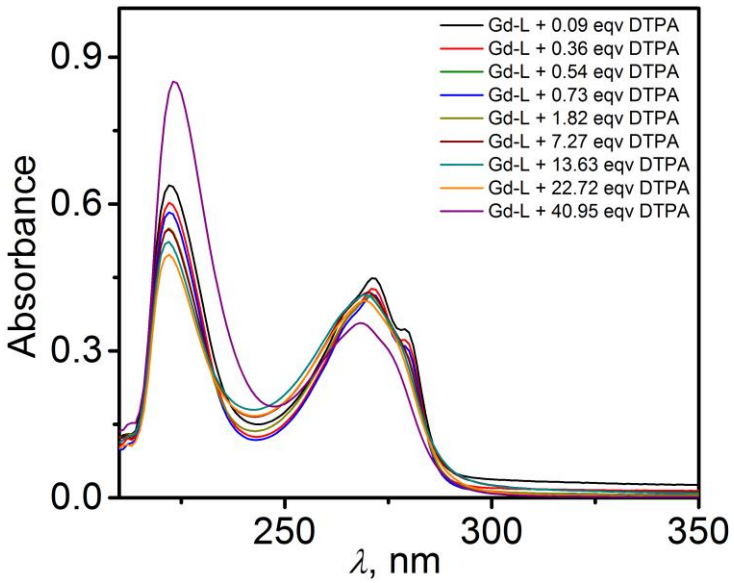

Figure S2. UV-Vis spectral changes during competitive study for determining pGd value for ligand H_2hbda (where, L = H_2hbda) against DTPA.

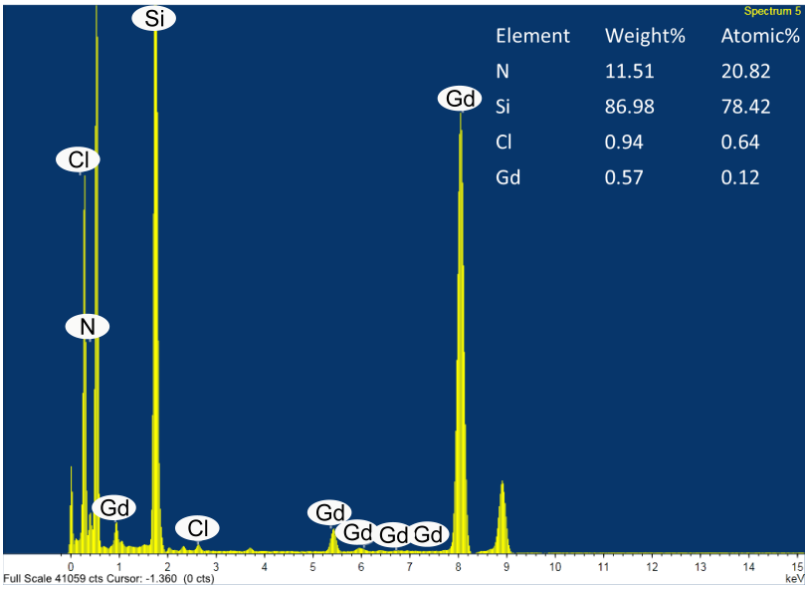

Figure S3. Energy dispersive X-ray (EDS) analysis of complex **1**@SiO_2NPs showing existence of Gd, Si, N and Cl elements in the isolated nanoparticles.

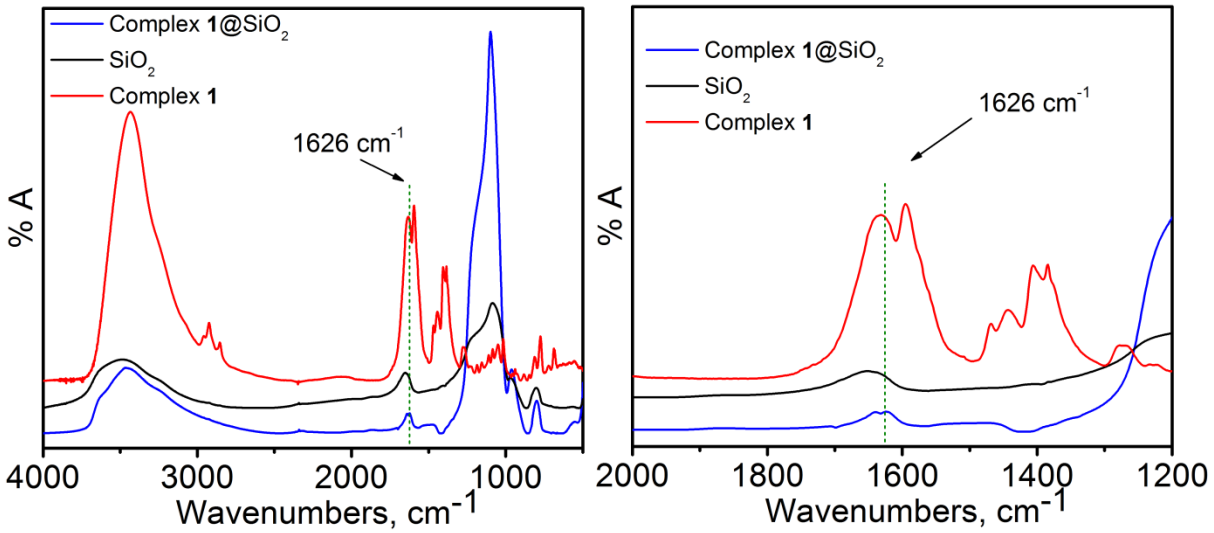

Figure S4. FTIR spectrum of complex **1**, complex **1**@SiO_2NP and SiO_2 NPs.

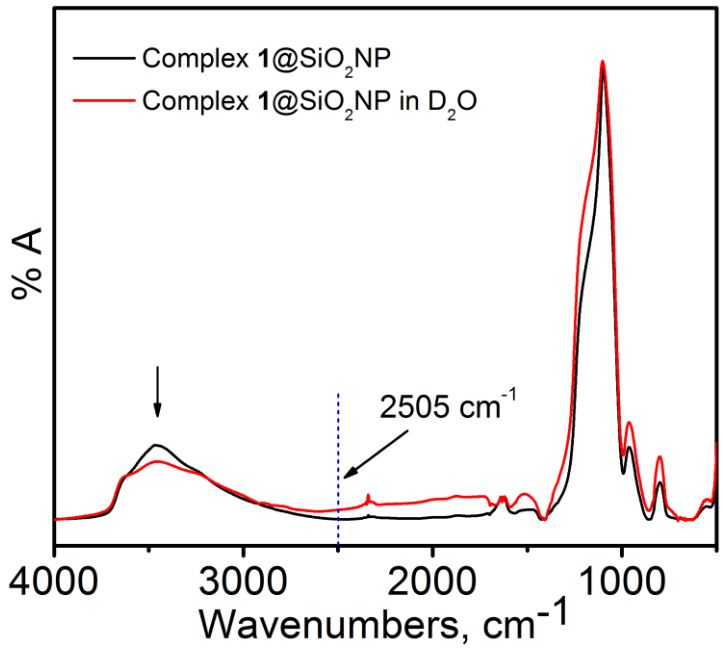

Figure S5. FTIR spectrum of complex **1**@SiO_2NP and complex **1**@SiO_2NP_D_2O. Normalized with respect to 1100 cm^{-1} band.

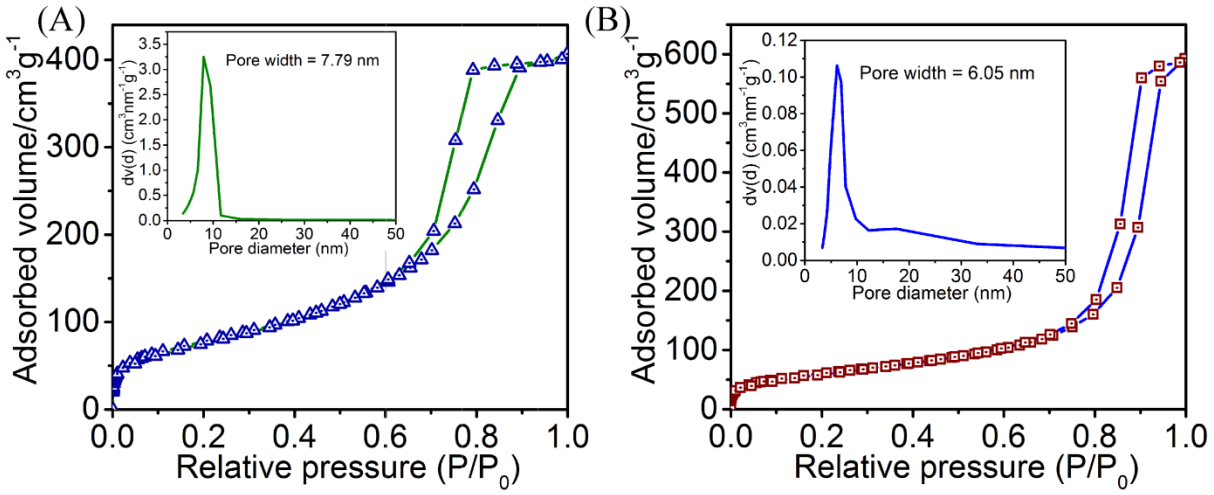

Figure S6. Nitrogen adsorption-desorption isotherm and pore size distribution (inset) of (A) pristine SiO_2NP, and (B) complex **1**@SiO_2NPs.

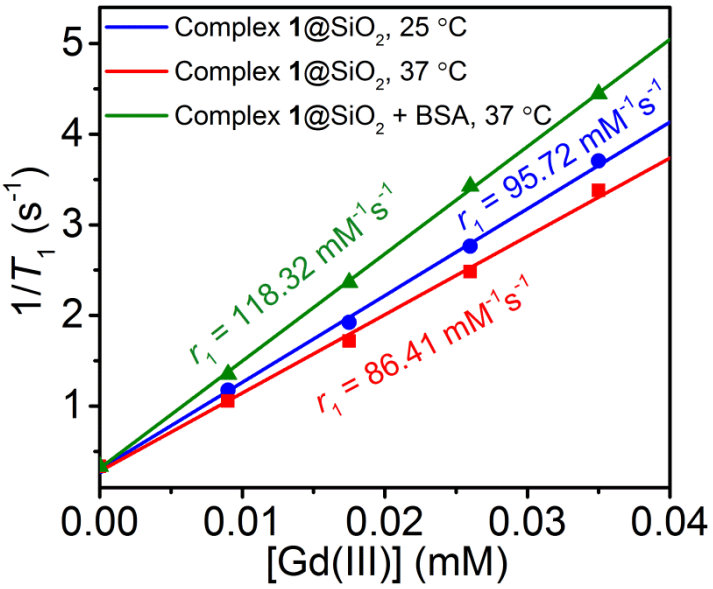

Figure S7. ($1/T_1$) *versus* **[**Gd(III)] for complex **1**@SiO_2NPs, recorded at 25 °C, 37 °C and in the presence of 4.5% (w/v) BSA. Measurements were done at pH ~ 7.4, and 1.41 T.

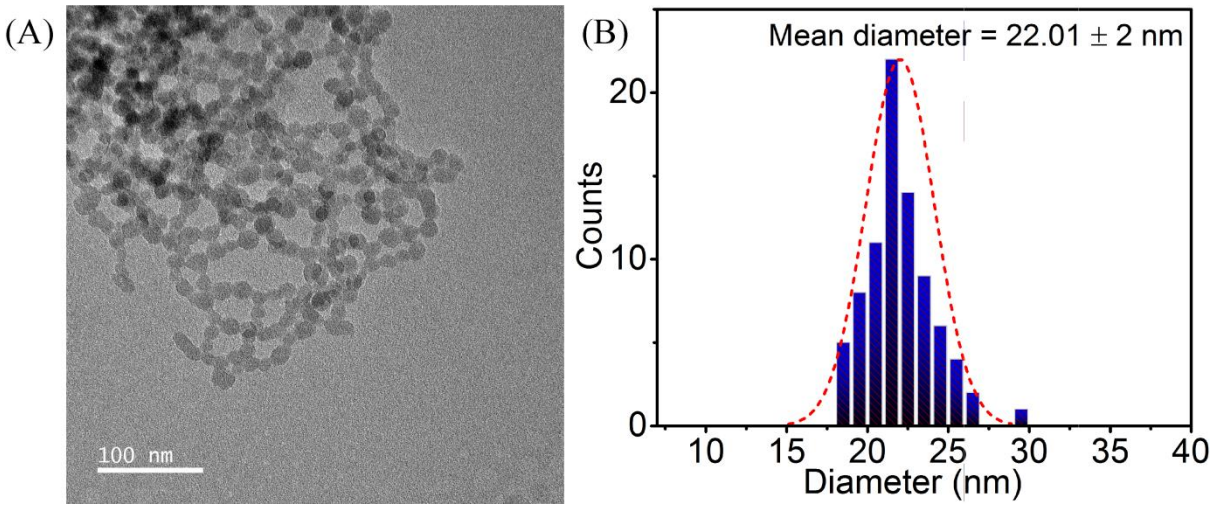

Figure S8. Morphological characterization of pristine SiO_2 nanoparticles (in the absence of complex **1**). (A) Representative TEM image and (B) corresponding particle size distribution plot.

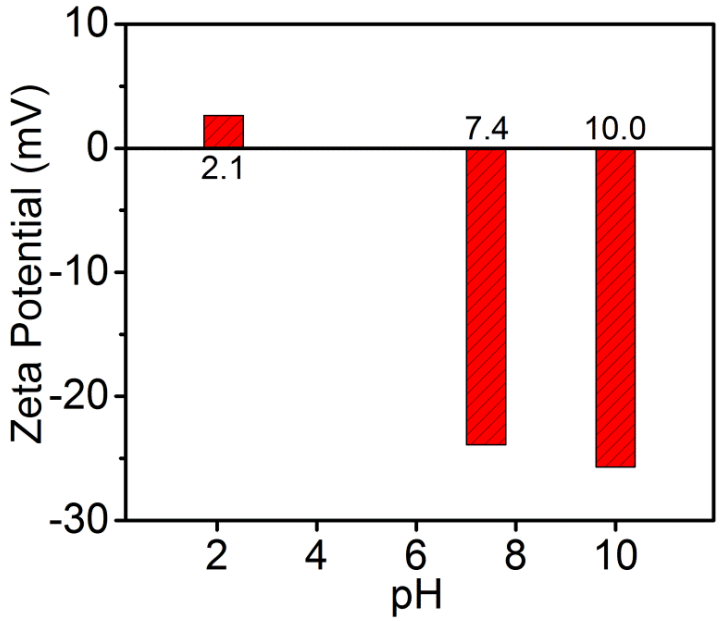

Figure S9. Zeta potentials of hollow porous pristine silica nanoparticles (in the absence of complex **1**) measured in the pH range 2 to 10.

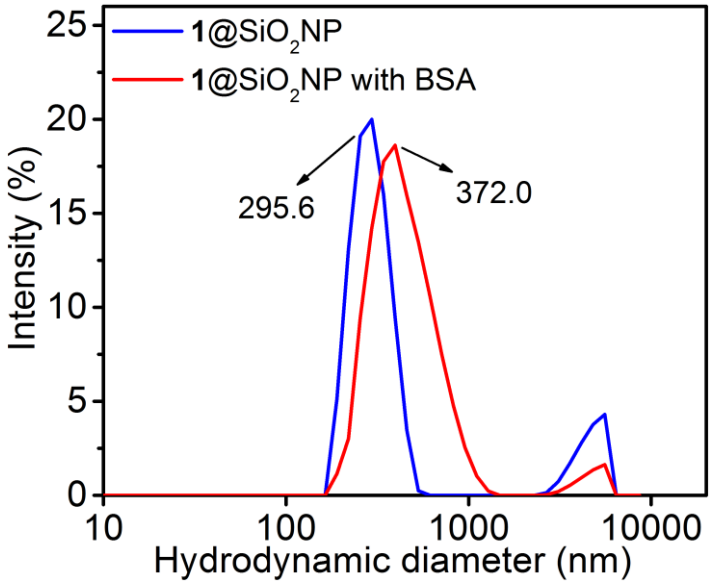

Figure S10. DLS hydrodynamic diameters of complex **1**@SiO_2NPs in the absence and the presence of BSA (4.5% w/v) at pH 7.4.

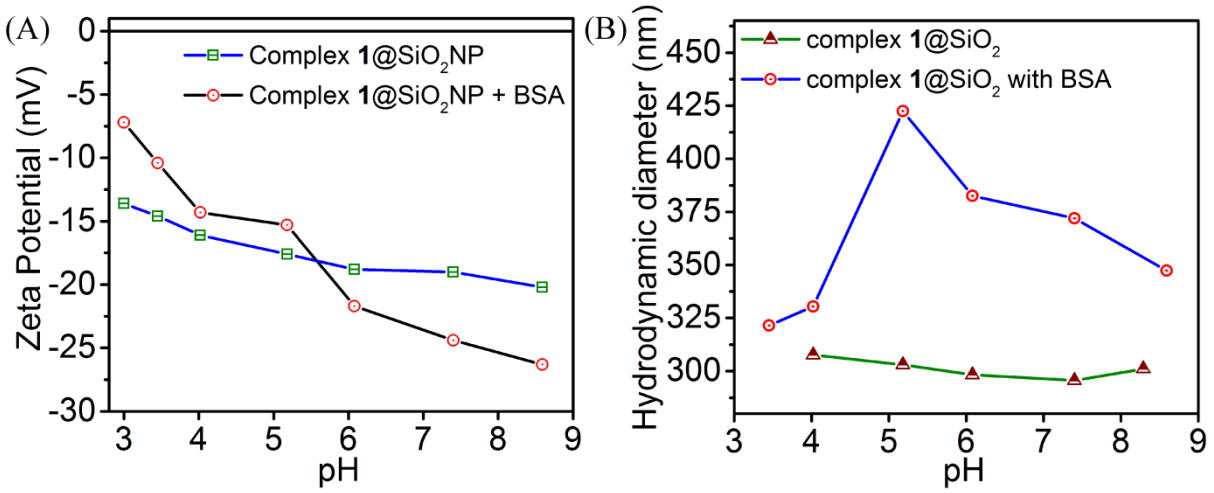

Figure S11: (A) Zeta potentials of complex **1**@SiO_2NP recorded in absence and presence of 4.5% (w/v) BSA at different pH. (B) Hydrodynamic diameter of complex **1**@SiO_2NP in absence and presence of 4.5 % (w/v) BSA at different pH.

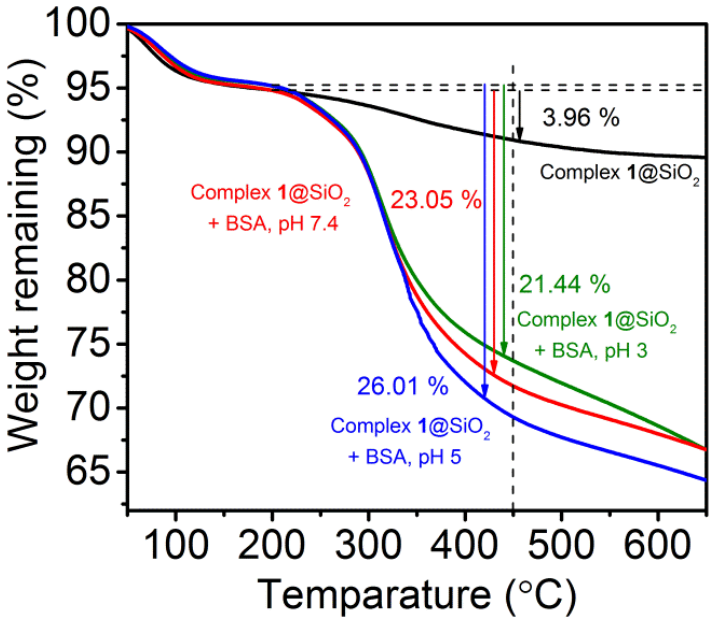

Figure S12: TGA analysis spectra for complex **1**@SiO_2NP (black line), in the presence of 4.5% (w/v) BSA at pH 3 (green line), pH 5 (blue line), and pH 7.4 (red line).

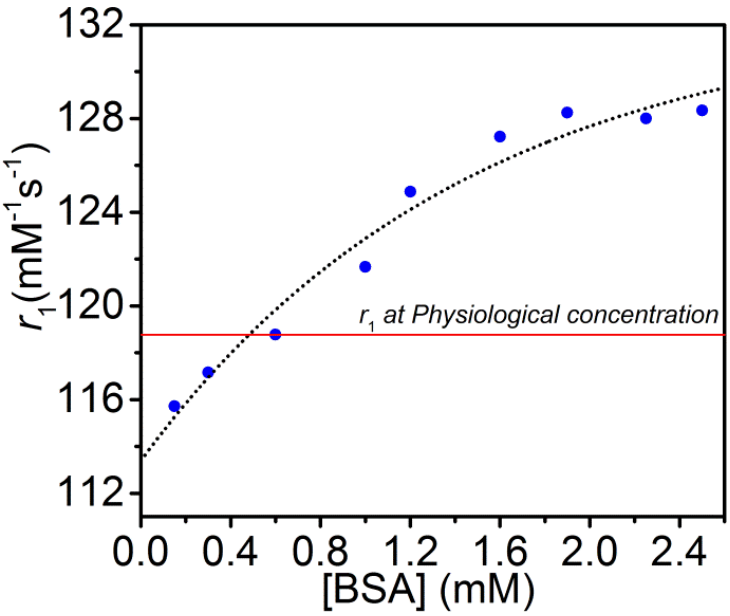

Figure S13: r_1 values for complex **1**@SiO_2 measured in presence of increasing concentration of BSA, at 37 °C, pH 7.4, and 1.41 T.

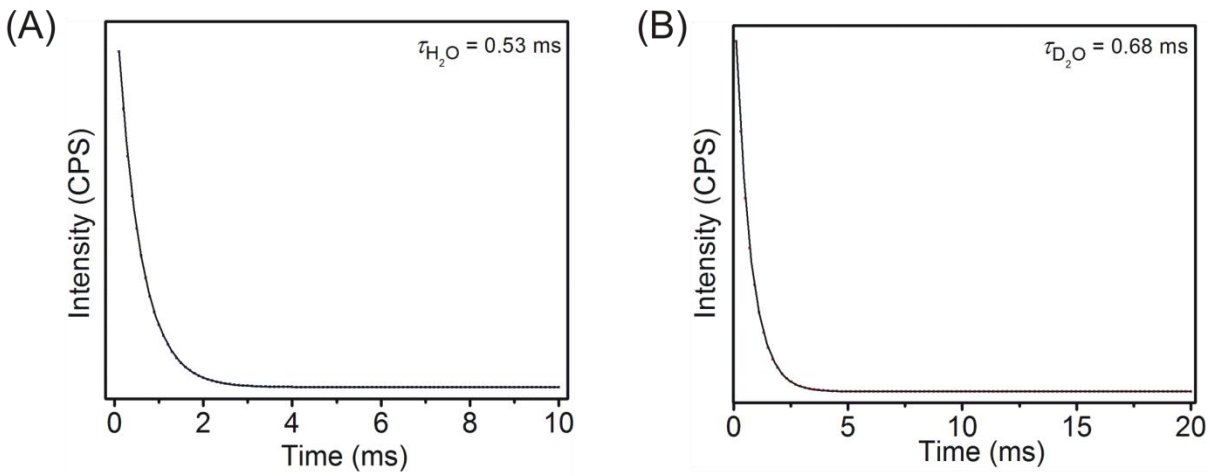

Figure S14. Luminescence lifetime decay curves of complex **2** in (A) H_2O, and (B) D_2O at pH ~ 10.0.

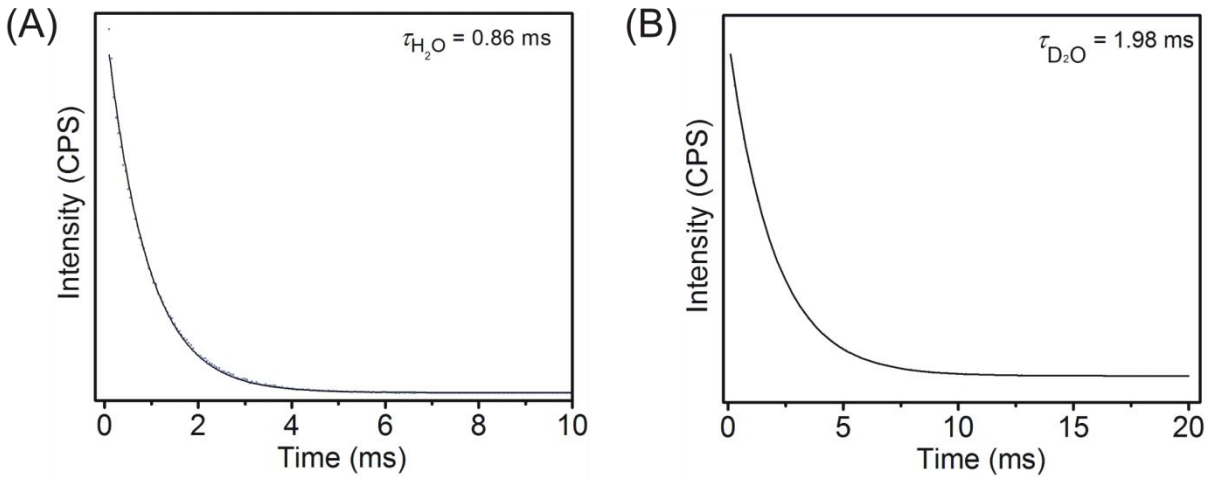

Figure S15. Luminescence lifetime decay curves of complex **2** in (A) H_2O, and (B) D_2O at pH ~ 4.0.

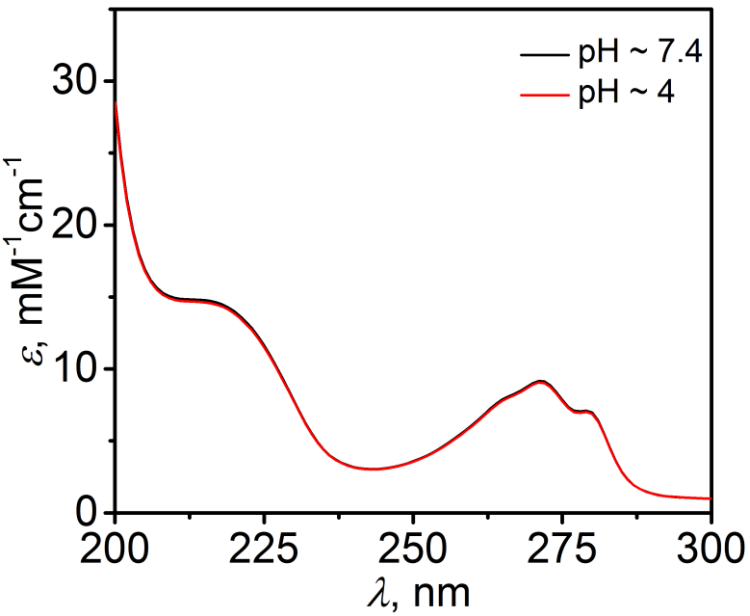

Figure S16. UV-Vis spectra of complex **1** at pH ~ 7.4, and 4.0.

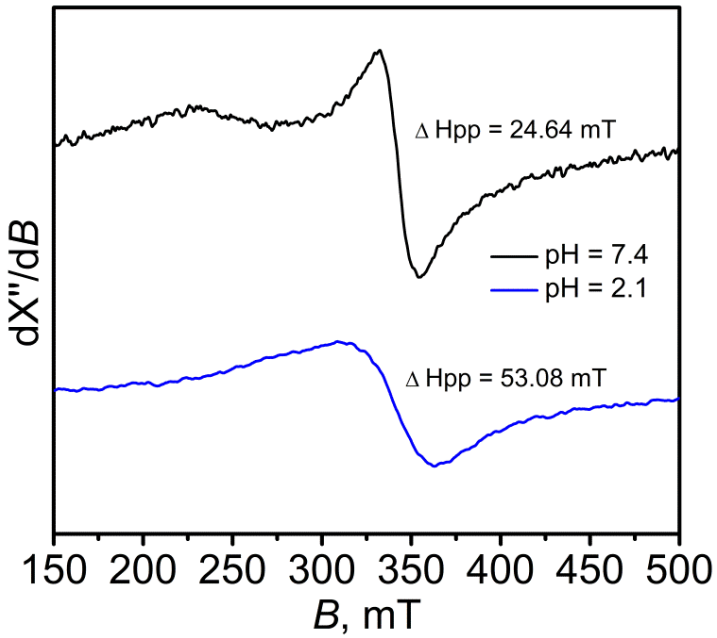

Figure S17. X-band EPR spectra of complex **1** at pH ~ 2.1, and 7.4; measured at room temperature, power = 0.995 mW, modulation frequency = 100 kHz, and amplitude = 10 G.

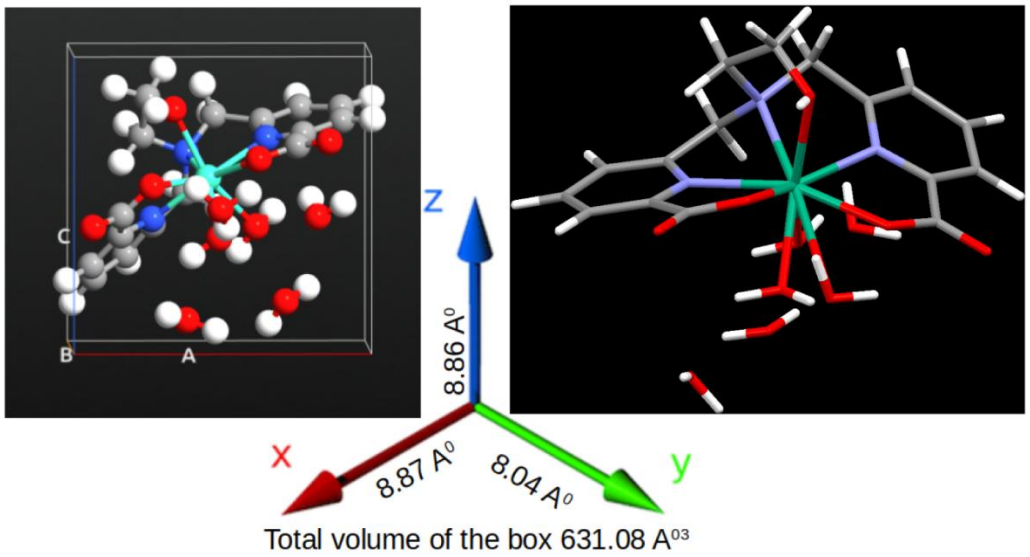

Figure S18. Optimized structure of tris(aquated) complex **1**. Optimized at B97D3 level containing a pure functional, B97. Red = oxygen, blue = nitrogen, grey = carbon, green = gadolinium, and white = hydrogen. According to the calculations the molecule could be fitted within a cavity having an estimated volume of 631.08 A°^{3} (i.e. 8.87A°×8.04A°×8.86A°).

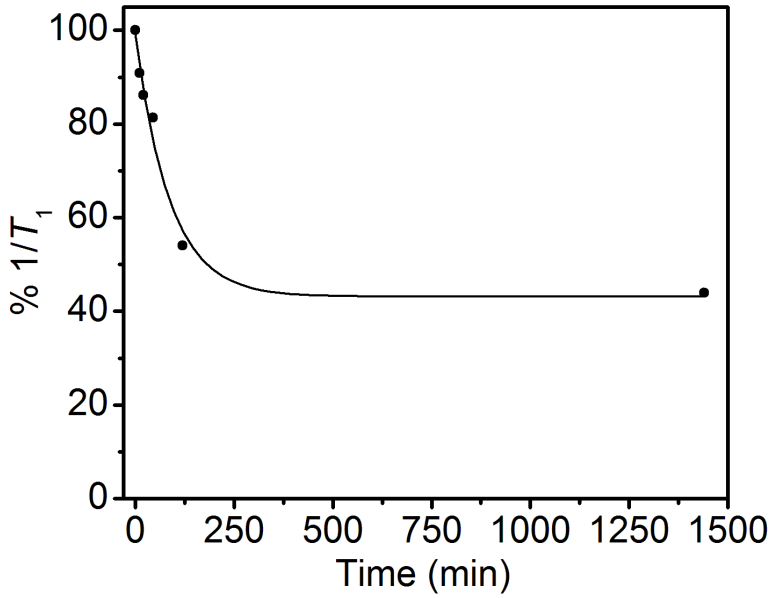

Figure S19. Time profile of transmetallation of $[Gd(hbda)(H_2O)_3]^+$ (complex **1**) with 1 equivalent of Zn(II) ion. It is monitored by measuring T_1 time as liberated Gd(III) ion precipitates as $GdPO_4$, which does not make contribution to T_1. The T_1 relaxation times were measured by adding 2.5 mM $ZnCl_2$ to 2.5 mM complex **1** in 50 mM phosphate buffer at 37 °C.

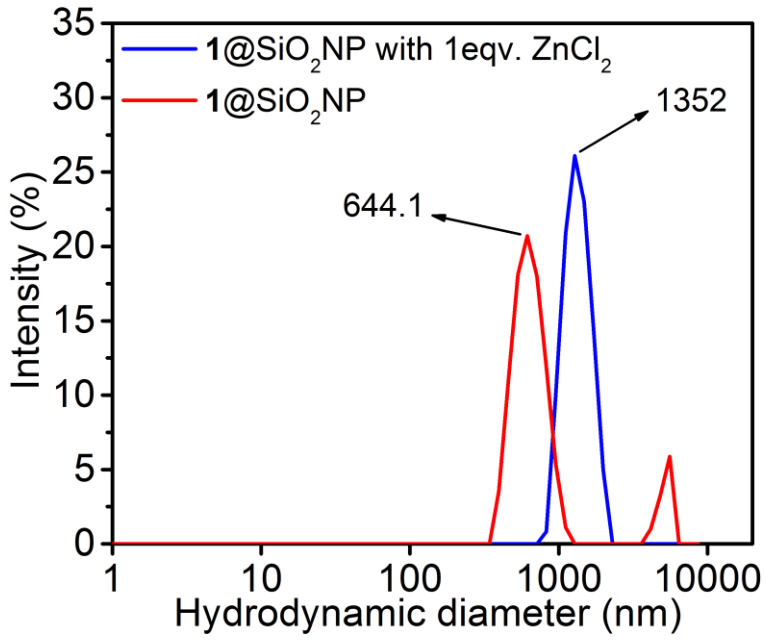

Figure S20. Hydrodynamic diameter of complex **1**@SiO_2NPs in the absence and the presence of equivalent amount of $ZnCl_2$, measured in phosphate buffer, at pH ~ 7.0.

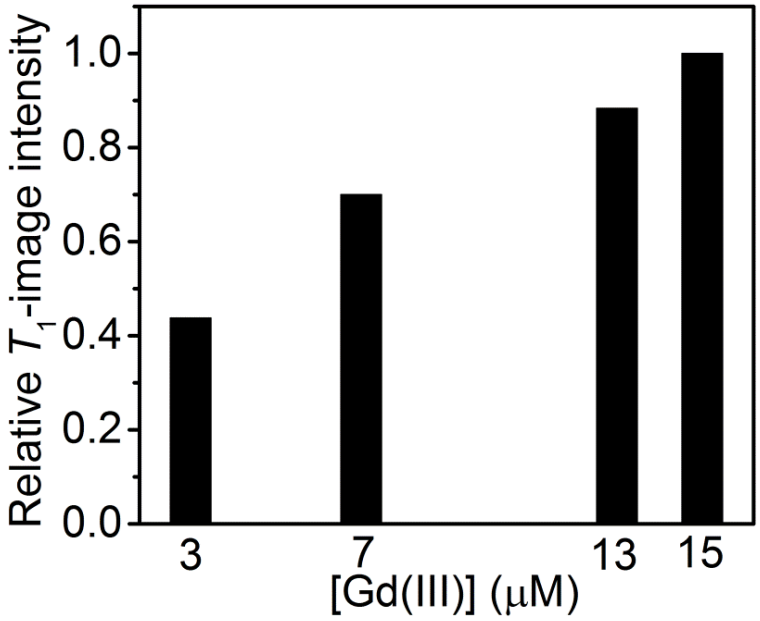

Figure S21. Relative image intensity plot for MR-images of complex **1**@SiO_2NPs using *ImageJ* software.

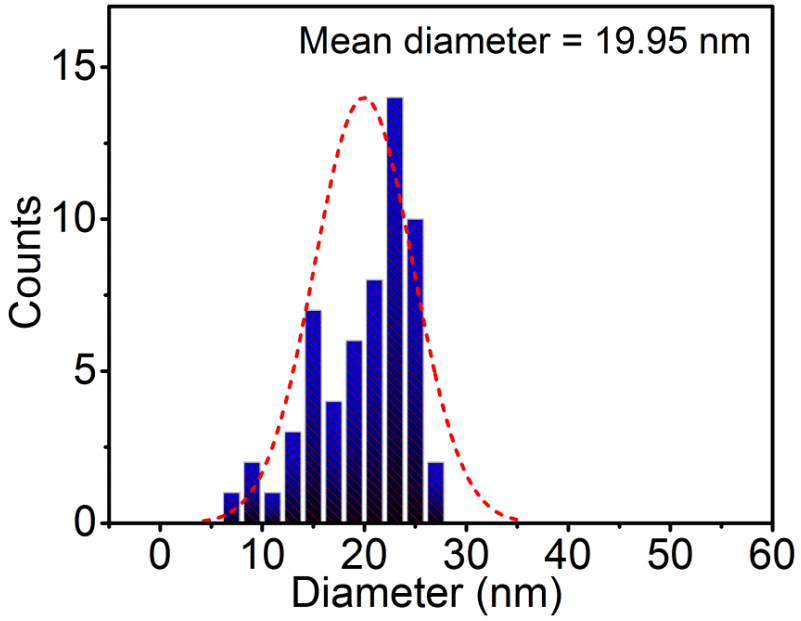

Figure S22. Particle size distribution of complex **1**@SiO_2NPs that was internalized inside HeLa cell after 48 hours.

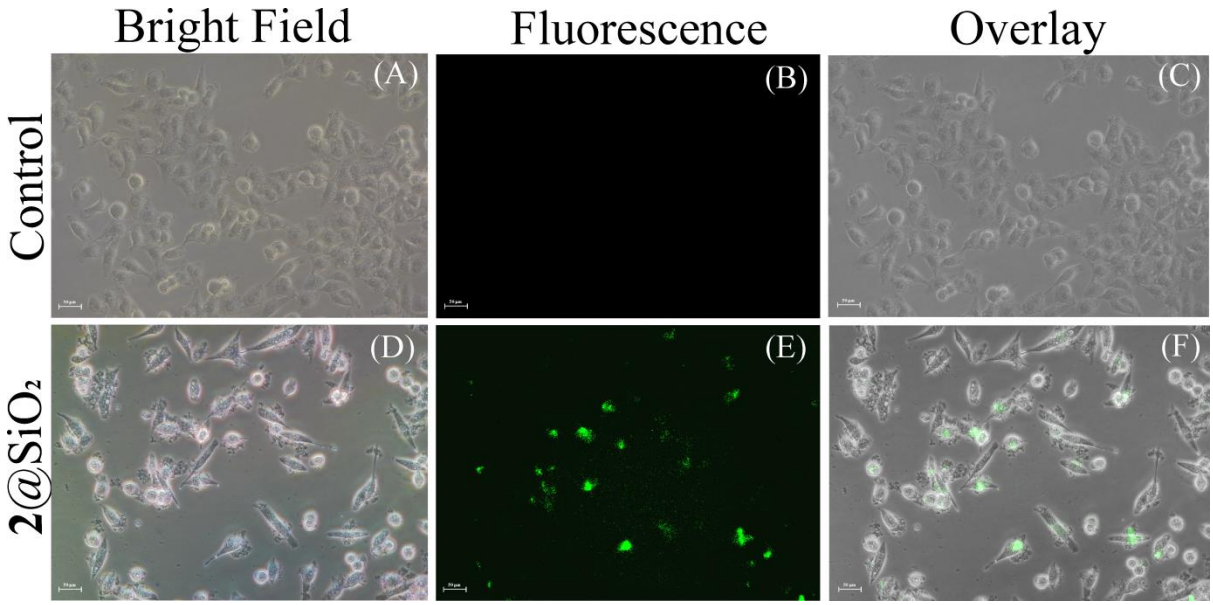

Figure S23: Fluorescence microscopy images of HeLa cells (A)-(C): untreated; (D)-(F): treated with complex **2**@SiO_2 *i.e.*, Tb(III)-congener. Cellular uptake was visualized by treating HeLa cells with 100 μM of complex **2**@SiO_2 for 24 h. Cells were subsequently fixed with 4% formaldehyde solution for 15 mins, thoroughly washed with PBS and then observed under Fluorescence inverted microscope *Nikon* ECLIPSE T*i*-U.

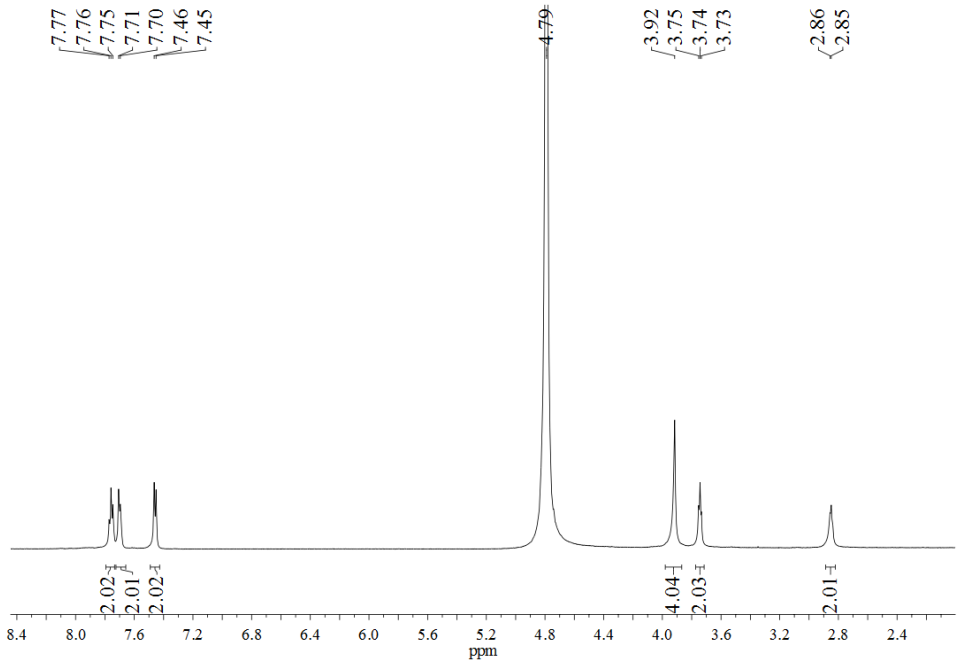

Figure S24. ^{1}H-NMR spectrum of ligand H_2hbda•HCl in D_2O solvent.

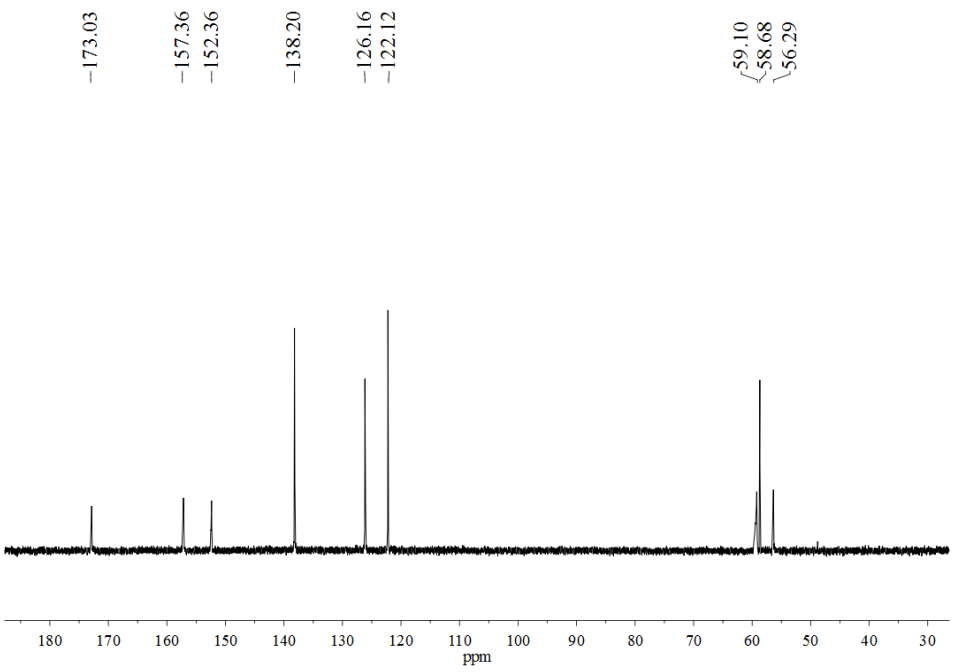

Figure S25. ^{13}C-NMR spectrum of ligand H_2hbda•HCl in D_2O solvent.

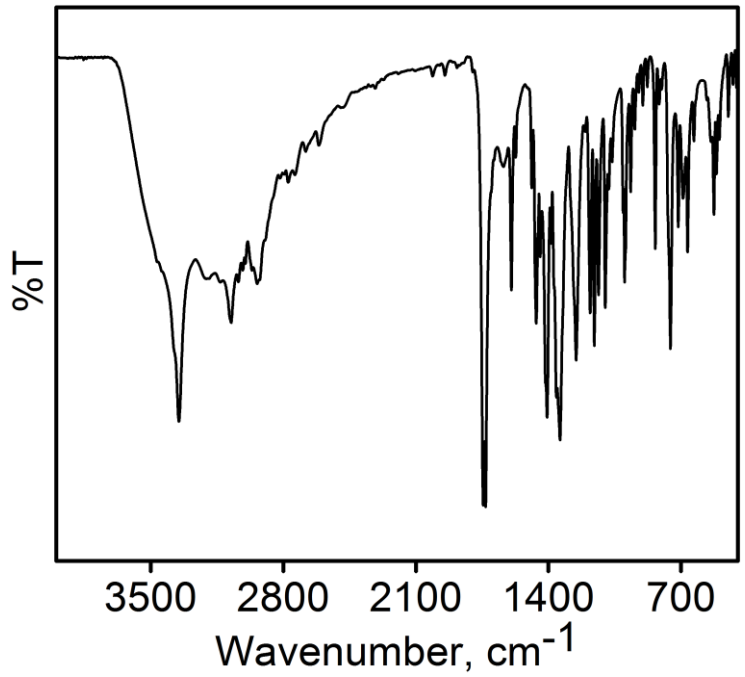

Figure S26. FTIR spectrum of ligand H_2hbda•HCl.

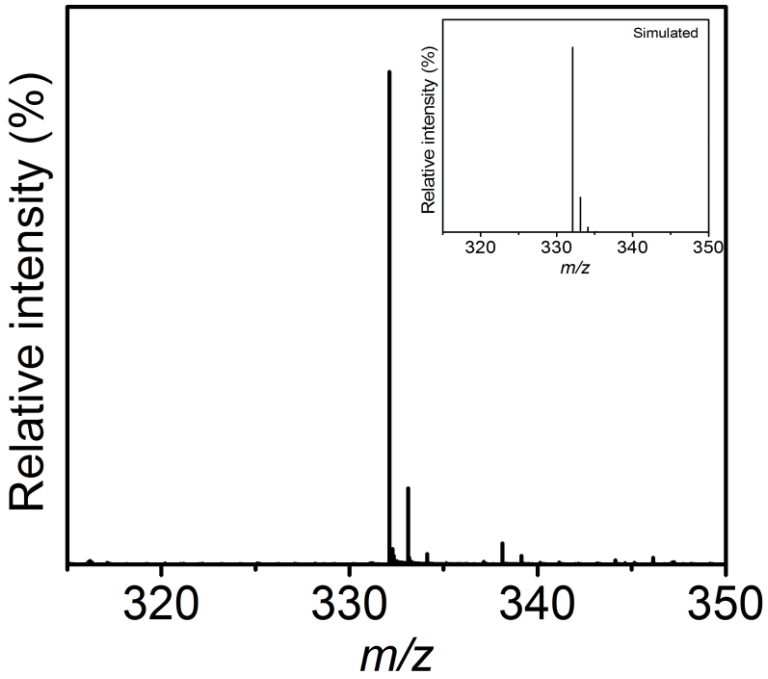

Figure S27. ESI-MS (+ve) mass spectrum of aqueous solution of ligand H_2hbda•HCl. Simulated spectrum has been given as inset.

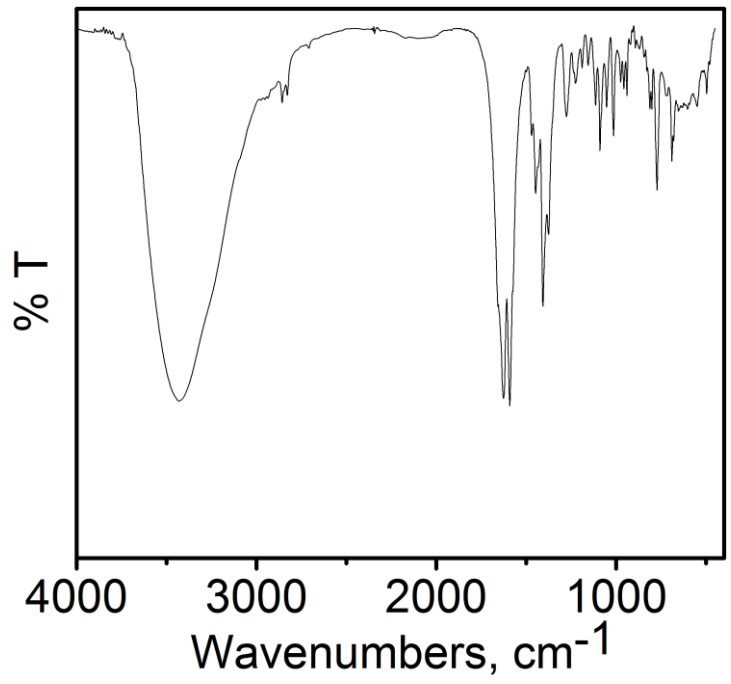

Figure S28. FTIR spectrum of complex **1**.

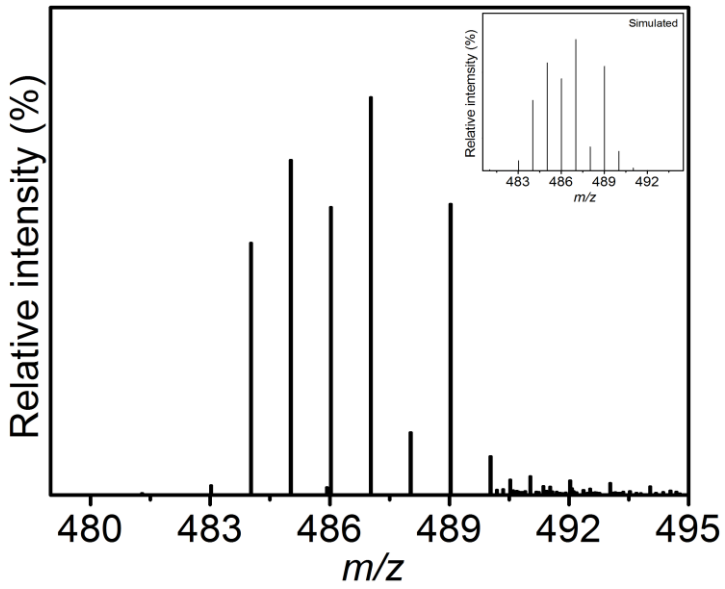

Figure S29. ESI-MS (+ve) mass spectrum of complex **1**. Simulated spectrum has been been given as inset.

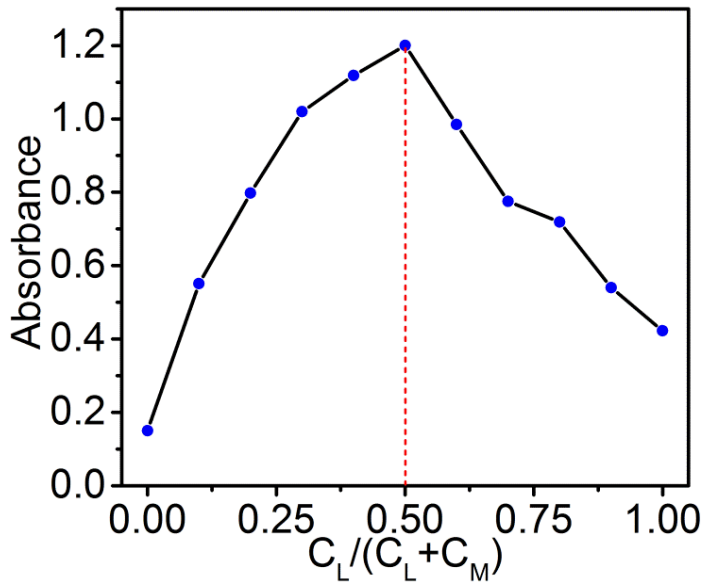

Figure S30: Job's plot for H_2hbda and Gd(III) by measuring absorbance from UV-Vis spectra, recorded by varying proportion of H_2hbda and Gd(III). [ligand] + [$GdCl_3 \bullet xH_2O$] = 0.5 mM, constant for all the solution. The dotted line corresponds to 1:1 stoichiometric ratio for complex **1** formation.

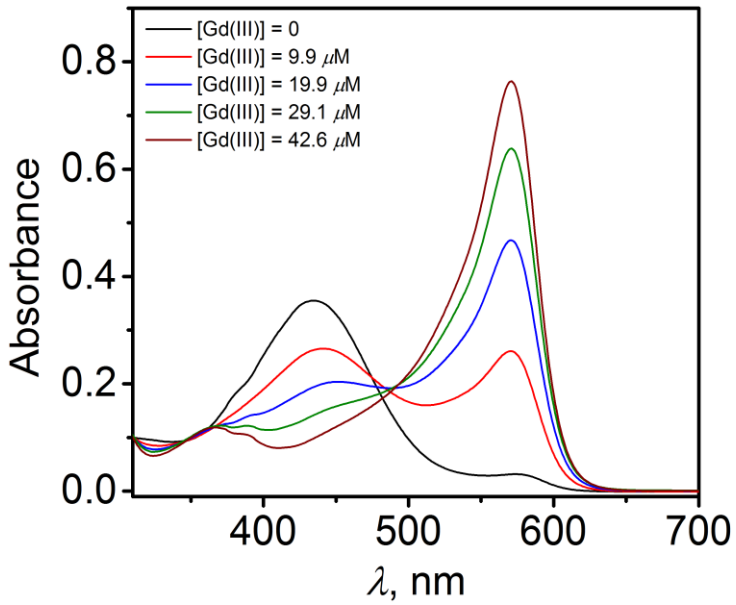

Figure S31. UV-Vis spectrum of xylenol orange solution in different concentrations of Gd(III) ion in acetate buffer at pH ~ 5.8.

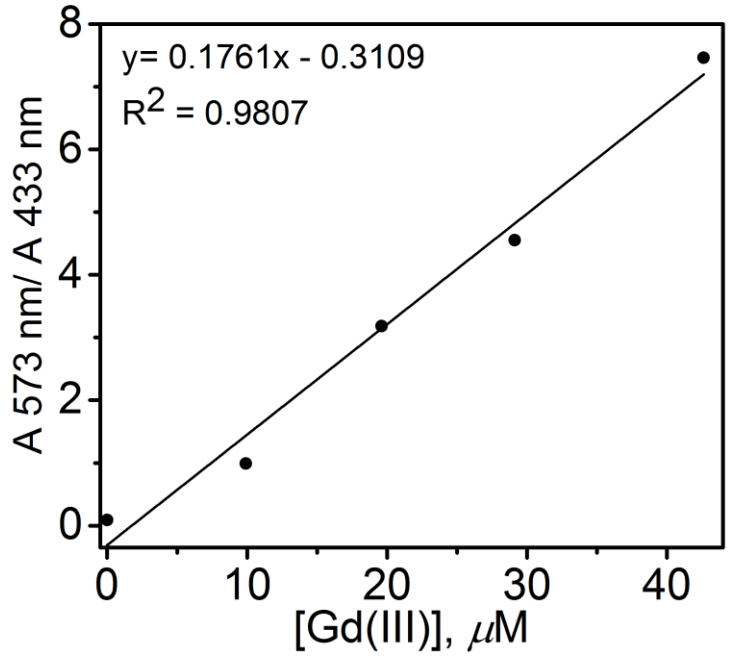

Figure S32. Calibration curve obtained from above observed changes in absorbances of xylenol orange in various concentrations of Gd(III) ions in acetate buffer at pH ~ 5.8. For 100 μL of [complex **1**] = 12.45 mM in 2 mL of xylenol orange solution observed A 573 nm/ A 433 nm = 0.23.

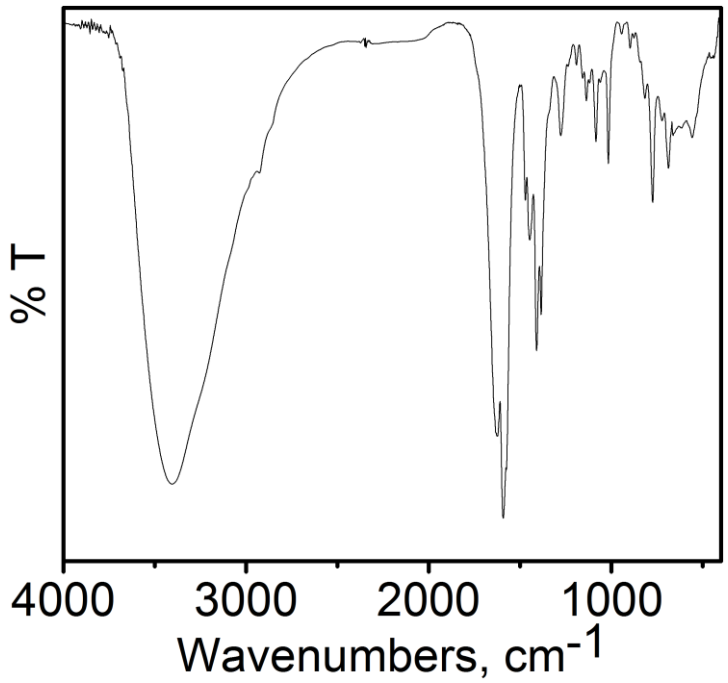

Figure S33. FTIR spectrum of complex **2**.

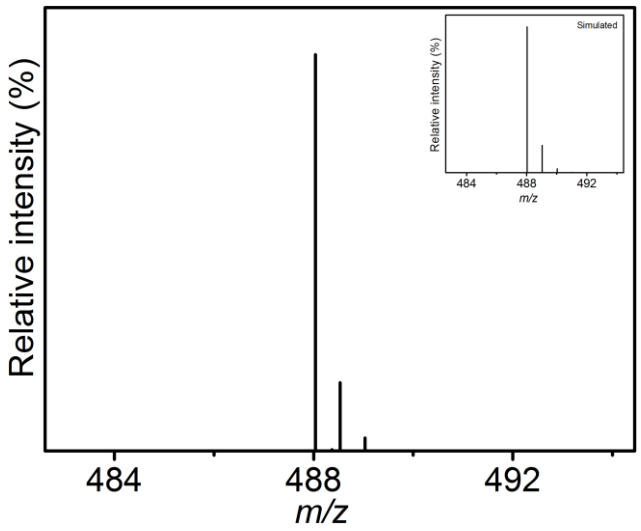

Figure S34. ESI-MS (+ve) mass spectrum of complex **2**. Simulated spectrum has been been given as inset.

Competition titration with DTPA:

The general procedure used to determine the affinity of any ligand for Gd(III) ion is by competition titration. Throughout the titration, pH, concentrations of ligand H_2hbda and Gd(III) ion were kept constant. Varying volumes of standardized H_5DTPA stock solution were added to solutions containing constant concentration of ligand (H_2hbda) and Gd(III) ion in constant electrolyte concentration. The pH of all solutions was maintained at 7.4 by preparing all

solutions in 10 mM HEPES buffer. All the solutions were kept for 48 hr to attain the thermodynamic equilibrium. The concentration of free and complexed ligand in each set of solution was determined from absorbance spectra considering a particular range of wavelength where spectral changes occurred. In that particular wave length range, variation of absorbance values for each solution set was calculated with respect to the absorbance of ligand H_2hbda (in that wavelength range). Then, the concentrations of Gdhbda complex, GdDTPA complex, free H_2hbda and free H_5DTPA for each set were calculated from the obtained values of variation of absorbances (calculated with respect to ligand absorbance). Then the logarithm values of respective ratios for GdDTPA to Gdhbda complex concentrations against logarithm values of ratios free H_5DTPA to free H_2hbda concentrations we plotted for each set of samples. Then we obtained a linear plot. From the linear plot, pGd value for the ligand H_2hbda was calculated as its x-intercept value based on the equation given below.

$\log([GdDTPA]/[Gdhbda] = \Delta pM + \log([H_5DTPA]/[H_2hbda]$

Number of Complexes per Nanoparticle:

The average number of complexes confined within each nanoparticle was determined using the formula:[1]

$$N_1 = \frac{cVN_A}{\eta/m_{NP}} = \frac{cVN_A(\frac{1}{6}\pi\rho_{NP}d^3)}{\eta}$$

Where c = concentration in mother suspension,

V = volume of mother suspension,

N_A = Avogadro's number,

η = yield from synthesis,

m_{NP} = mass of nanoparticle,

ρ_{NP} = density of nanoparticle (considered same as that of pure silica, 1.95 g cm^{-3}),

d = diameter of nanoparticle.

500 µL of mother suspension was lyophilized for 24 h and 14 mg of dry silica were obtained. For Gd(III) concentration to be 0.088 mM and each nanoparticle sized 23.4 nm, n_{cplx} = 20.

Computational Details:

The DFT calculations are performed using Gaussian16 package.[2] The initial geometries of the complexes were optimized at B97D3 level containing a pure functional, B97,[3] with the Grimme's D3BJ[4] dispersion (B97D3). Here, we have used correlation-consistent double-zeta (cc-pVDZ) basis sets developed by Dunning and coworkers[5] for the all the atoms except Gd. LANL2DZ (Los Alamos National Laboratory 2 Double-Zeta), ECP type basis set was used to model the metal atom.[6] The effect of water as solvent in the calculations was taken care through SCRF (self-consistent reaction field)[7] approach using CPCM[8] (polarizable conductor calculation model) formalism, as implemented in Gaussian16. Subsequent frequency analysis of the optimized geometries was performed to ensure the global minima in the potential energy surfaces for the system.

Table S1. Textural properties of blank SiO_2NP and complex **1**@SiO_2NP.

	BET surface area (m^2/g)	Pore volume (cc/g)
Blank SiO_2NP	281.70	1.65
Complex **1**@SiO_2NP	269.61	1.19

Table S2. Relaxivity data of complex **1**@SiO_2NPs (per Gd), at 1.41 T, 25 °C, and pH ~ 7.4. Concentration of Gd(III) in the suspension determined by ICP-MS and bulk magnetic susceptibility (BMS) mechanism.

Sets	r_1 **(ICP-MS)**	r_1 **(BMS)**
I.	94.27	94.01
II.	95.72	
III.	97.07	

Hence, nanoparticles can be synthesized within ± 2% reproducibility limit.

To understand if the silica matrix had any contribution to relaxivity values, blank silica nanoparticles was prepared following same procedure with water as doping solution.

Synthesized nanoparticles was suspended in HEPES solution, pH ~ 7.4 and T_1 and T_2, measured at 1.41 T, were 2970 ms and 2986 ms respectively which is same as that of water.

Table S3: Relaxivity of some Gd-based contrast agents.

Gd-based Contrast agents	***q***	***r*$_1$ (mM^{-1}s^{-1}), at pH 7.4**	**Ref. No. in SI**
Complex **1**	3	9.82, at 25 °C, 1.41 T 9.05, at 37 °C, 1.41 T	This work
[Gd(cbda)(OH$_2$)$_3$]	3	10.95, at 25 °C, 1.41 T	9
Gd(dpaa)(H$_2$O)$_3$]	3	9.4, at 25 °C, 1.06 T	10
[Gd(dhqN-SO$_3$)(H$_2$O)$_3$]$^{3-}$	3	9.25, at 37 °C, 1.2 T	11
Gd(edta)(H$_2$O)$_3$]$^-$	3	7.15, at 25 °C, 0.47 T	12
Complex **1**@SiO$_2$NP	3	86.41, at 37 °C, 1.41 T 95.3, at 25 °C, 1.41 T	This work
[Gd(TCAS)]- SN-III	—	46.49, at 37 °C, 1.41 T 50.91, at 25 °C, in presence of BSA	13
MSN-Gd	2	28.8, at 3 T	14
PSS-Na[Gd·2]	2.65	12.41, at 25 °C, 0.47 T	15
Si25NPs	3	77, at 37 °C, 1.2 T	11
GdDOTA⊂NPs	1	72.3, at 37 °C, 1.41 T	16
FSb-EuGd	—	38.8 at 25 °C, 9.4 T	17
Gd$_2$O$_3$@MSN	—	45.08 at 0.5 T	18
Gd@SiO2–PEG500	—	18.5, at 40 °C, 1.41 T	19
Gd^{3+} -incorporated MSN	—	51.85 at 0.5 T	20

Table S4. DLS hydrodynamic diameters and zeta potentials of complex **1**@SiO_2NPs in absence and presence of BSA, at pH ~ 7.4.

Particles	**Hydrodynamic diameter (nm)**	**PdI**	**Zeta Potential (mV)**
Complex **1**@SiO_2	295.6	0.365	-19.0
Complex **1**@SiO_2 + 4.5 % BSA (w/v)	372.0	0.471	-24.6

Table S5. DLS hydrodynamic diameters, FE-TEM particle size and longitudinal relaxivity values of bare silica nanoparticles, complex **1**@SiO_2NPs in the absence and the presence of BSA, and in different pH solutions.

Material	**Hydrodynamic diameter (nm)**	**PdI**	**Particle Size (nm)**	**r_1 ($mM^{-1}s^{-1}$) at 37 °C, pH ~ 7.4, 1.41 T**
SiO_2 NP	284.1	0.256	22.0	—
Complex **1**@SiO_2	295.6	0.365	23.4	86.41
Complex **1**@SiO_2 + 4.5 % BSA (w/v)	372.0	0.471	24.4	118.32
Complex 1@SiO_2 at different pH	**Hydrodynamic diameter (nm)**	**PdI**	**r_1 ($mM^{-1}s^{-1}$) at 25 °C, 1.41 T**	
4.02	307.6	0.327	95.81	
5.18	303.0	0.312	95.97	
6.08	298.3	0.276	95.61	
7.40	295.6	0.365	95.32	
8.29	301.1	0.302	95.44	

Table S6: Optimized coordinates of the complex **1** at B97D3 level of theory. (in xyz format)

C -4.040000e+00 7.000000e-01 -3.385000e+00

C -3.168000e+00 2.500000e-01 -2.450000e+00

N -2.222000e+00 1.037000e+00 -2.010000e+00

C -2.168000e+00 2.292000e+00 -2.234000e+00

C -2.963000e+00 2.861000e+00 -3.171000e+00

C -3.927000e+00 2.044000e+00 -3.797000e+00

C -3.186000e+00 -1.154000e+00 -1.807000e+00

O -2.285000e+00 -1.405000e+00 -9.280000e-01

O -4.052000e+00 -2.011000e+00 -2.123000e+00

C -1.171000e+00 3.022000e+00 -1.318000e+00

N -1.181000e+00 2.191000e+00 -9.700000e-02

C -3.430000e-01 2.728000e+00 9.930000e-01

C 1.094000e+00 2.241000e+00 8.440000e-01

N 1.192000e+00 1.049000e+00 3.880000e-01

C 2.272000e+00 3.230000e-01 5.450000e-01

C 3.445000e+00 8.890000e-01 9.300000e-01

C 3.455000e+00 2.263000e+00 1.239000e+00

C 2.233000e+00 2.956000e+00 1.222000e+00

C 2.064000e+00 -1.174000e+00 2.780000e-01

O 2.994000e+00 -2.007000e+00 4.390000e-01

O 9.030000e-01 -1.536000e+00 -1.070000e-01

C -2.501000e+00 2.025000e+00 4.160000e-01

Gd -5.700000e-01 9.500000e-02 -7.420000e-01

O 8.750000e-01 9.960000e-01 -2.243000e+00

O 2.766000e+00 2.593000e+00 -2.029000e+00

O -2.740000e-01 -1.359000e+00 -2.460000e+00

C -2.357000e+00 1.035000e+00 1.613000e+00

O -1.602000e+00 -5.200000e-02 1.306000e+00

H -4.790000e+00 5.700000e-02 -3.796000e+00

H -2.867000e+00 3.897000e+00 -3.424000e+00

H -4.564000e+00 2.437000e+00 -4.561000e+00

H -1.940000e-01 3.068000e+00 -1.752000e+00

H -1.498000e+00 4.020000e+00 -1.113000e+00

H -6.780000e-01 2.323000e+00 1.925000e+00

H -4.280000e-01 3.795000e+00 1.013000e+00

H 4.339000e+00 3.060000e-01 9.970000e-01

H 4.367000e+00 2.763000e+00 1.490000e+00

H 2.176000e+00 3.988000e+00 1.498000e+00

H -3.116000e+00 1.597000e+00 -3.480000e-01

H -2.936000e+00 2.950000e+00 7.330000e-01

H 3.810000e-01 1.382000e+00 -2.971000e+00

H 1.398000e+00 1.678000e+00 -1.815000e+00

H 3.511000e+00 2.143000e+00 -1.623000e+00

H 2.581000e+00 3.403000e+00 -1.548000e+00

H -7.200000e-02 -2.230000e+00 -2.111000e+00

H -1.077000e+00 -1.402000e+00 -2.985000e+00

H -1.869000e+00 1.535000e+00 2.424000e+00

H -3.338000e+00 7.290000e-01 1.910000e+00

O -1.259000e+00 -1.851000e+00 -4.885000e+00

H -1.825000e+00 -2.599000e+00 -4.680000e+00

H -4.030000e-01 -2.170000e+00 -5.181000e+00

O -2.780000e-01 -3.163000e+00 -1.518000e+00

H 5.560000e-01 -3.165000e+00 -1.042000e+00

H -9.900000e-01 -2.939000e+00 -9.140000e-01

O 1.771000e+00 1.429000e+00 -4.499000e+00

H 1.287000e+00 1.914000e+00 -5.170000e+00

H 2.430000e+00 2.003000e+00 -4.101000e+00

H -2.157000e+00 -8.350000e-01 1.323000e+00

REFERENCES:

1. S. V. Eliseeva, B. Song, C. D. B. Vandevyver, A. -S. Chauvin, J. B. Wacker and J. C. G. Bunzli, *New. J. Chem*., 2010, **34**, 2915-2921.

2. M. J. Frisch, G. W. Trucks, H. B. Schlegel, G. E. Scuseria, M. A. Robb, J. R. Cheeseman, G. Scalmani, V. Barone, B. Mennucci, G. A. Petersson, H. Nakatsuji, M. Caricato, X. Li, H. P. Hratchian, A. F. Izmaylov, J. Bloino, G. Zheng, J. L. Sonnenberg, M. Hada, M. Ehara, K. Toyota, R. Fukuda, J. Hasegawa, M. Ishida, T. Nakajima, Y. Honda, O. Kitao, H. Nakai, T. Vreven, J. A., Jr. Montgomery, J. E. Peralta, F. Ogliaro, M. Bearpark, J. J. Heyd, E. Brothers, K. N. Kudin, V. N. Staroverov, R. Kobayashi, J. Normand, K. Raghavachari, A. Rendell, J. C. Burant, S. S. Iyengar, J. Tomasi, M. Cossi, N. Rega, J. M. Millam, M. Klene, J. E. Knox, J. B. Cross, V. Bakken, C. Adamo, J. Jaramillo, R. Gomperts, R. E. Stratmann, O. Yazyev, A. J. Austin, R. Cammi, C. Pomelli, J. W. Ochterski, R. L. Martin, K. Morokuma, V. G. Zakrzewski, G. A. Voth, P. Salvador, J. J. Dannenberg, S. Dapprich, A. D. Daniels, O. Farkas, J. B. Foresman, J. V. Ortiz, J. Cioslowski and D. J. Fox, Gaussian 09, Revision D.01; Gaussian, Inc.: Wallingford, CT, 2015.

3. A. D. Becke, Density-functional thermochemistry. V. *J. Chem. Phys.* 1997, **107**, 8554-8560.

4. S. Grimme, S. Ehrlich and L. Goerick, *J. Comput. Chem.* 2011, **32**, 1456-1465.

5. T. H. Dunning, *J. Chem. Phys.* 1989, **90**, 1007-1023.

6. P. J. Hay and W. R. *J.* Wadt, *Chem. Phys*. 1985, **82**, 299.

7. S. Meirtuš, E. Scorocco and J. Tomasi, *Chem. Phys*. 1981, **55**, 117-129.

8. V. Barone and M. Cossi, *J. Phys. Chem*. *A* 1998, **102**, 1995-2001.

9. M. Khannam, S. K. Sahoo and C. Mukherjee, *Eur. J. Inorg. Chem.*, 2019, 2518–2523.

10. A. M. Nonat, C. Gateau, P. H. Fries, L. Helm and M. Mazzanti, *Eur. J. Inorg.Chem*., 2012, 2049-206.

11. M. M. Karimdjy, G. Tallec, P. H. Fries, D. Imbert and M. Mazzanti, *Chem. Commun*. 2015, **51**, 6836-6838.

12. A. C. Chang, H. G. Brittain, J. Telser and M. W. Tweedle, *Inorg. Chem*. 1990, **29**, 4468–4473.

13. S. V. Fedorenko, S. L. Grechkina, A. R. Mustafina, K. V. Kholin, A. S. Stepanov, I. R. Nizameev, I. E. Ismaev, M. K. Kadirov, R. R. Zairov, A. N. Fattakhova, R. R. Amirov and S. E. Soloveva, *Colloids Surf. B: Biointerfaces* 2017, **149**, 243-249.

14. M. L. T. Kathryn, J. S. Kim, W. J. Rieter, H. An, W. Lin and W. Lin, *J. Am. Chem. Soc*. 2008, **130**, 2154-2155.

15. R. Zairov, G. Khakimullina, S. Podyachev, I. Nizameev, G. Safiullin, R. Amirov. A. Vomiero and A. Mustafina, *Sci. Rep*., 2017, **7**, 14010.

16. T. Courant, V. G. Roullin, C. Cadiou, M. Callewaert, M. C. Andry, C. Portefaix, C. Hoeffel, M. C. de Goltstein, M. Port, S. Laurent, L.V. Elst, R. Muller, M. Molinari and F. Chuburu, *Angew. Chem. Int. Ed*. 2012, **51**, 9119-9122.

17. S. L. C. Pinho, J. Sereno, A. J. Abrunhosa, M. H. Delville, J. Rocha, L. D. Carlos and C. F. G. C. Geraldes, *Inorg. Chem.* 2019, **58**, 16618−16628.

18. K. Ni, Z. Zhao, Z. Zhang, Z. Zhou, L. Yang, L. Wang, H. Ai and J. Gao, *Nanoscale* 2016, **8**, 3768–3774.

19. W. I. Lin, C. Y. Lin, Y. S. Lin, S. H. Wu, Y. R. Huang, Y. Hung, C. Chang and C. Y. Mou, *J. Mater. Chem. B* 2013, **1**, 639-645.

20. Z. Li, J. Guo, M. Zhang, G. Li and L. Hao, *Front. Chem*. 2022, **10**, 837032.